Advanced Composite Materials
Publication details, including instructions for authors and subscription information:
http://www.tandfonline.com/loi/tacm20

Monitoring of a CFRP-Stiffened Panel Manufactured by VaRTM Using Fiber-Optic Sensors

Shin-Ichi Takeda [a], Tadahito Mizutani [b], Takafumi Nishi [c], Naoki Uota [d], Yoshiyasu Hirano [e], Yutaka Iwahori [f], Yosuke Nagao [g] & Nobuo Takeda [h]

[a] Institute of Aerospace Technology, Japan Aerospace Exploration Agency, Japan

[b] Graduate School of Frontier Sciences, The University of Tokyo, Japan

[c] Graduate School of Frontier Sciences, The University of Tokyo, Japan

[d] KADO Corporation, Japan

[e] Institute of Aerospace Technology, Japan Aerospace Exploration Agency, Japan

[f] Institute of Aerospace Technology, Japan Aerospace Exploration Agency, Japan

[g] Institute of Aerospace Technology, Japan Aerospace Exploration Agency, Japan

[h] Graduate School of Frontier Sciences, The University of Tokyo, Japan

Version of record first published: 02 Apr 2012.

///VSP///

Advanced Composite Materials 17 (2008) 125–137

ADVANCED COMPOSITE MATERIALS
www.brill.nl/acm

Monitoring of a CFRP-Stiffened Panel Manufactured by VaRTM Using Fiber-Optic Sensors

Shin-ichi Takeda [a,*], **Tadahito Mizutani** [b], **Takafumi Nishi** [b], **Naoki Uota** [c], **Yoshiyasu Hirano** [a], **Yutaka Iwahori** [a], **Yosuke Nagao** [a] **and Nobuo Takeda** [b]

[a] Institute of Aerospace Technology, Japan Aerospace Exploration Agency, Japan
[b] Graduate School of Frontier Sciences, The University of Tokyo, Japan
[c] KADO Corporation, Japan

Received 31 January 2007; accepted 29 August 2007

Abstract

FBG (Fiber Bragg Grating) sensors and optical fibers were embedded into CFRP dry preforms before resin impregnation in VaRTM (Vacuum-assisted Resin Transfer Molding). The embedding location was the interface between the skin and the stringer in a CFRP-stiffened panel. The reflection spectra of the FBG sensors monitored the strain and temperature changes during all the molding processes. The internal residual strains of the CFRP panel could be evaluated during both the curing time and the post-curing time. The temperature changes indicated the differences between the dry preform and the outside of the vacuum bagging. After the molding, four-point bending was applied to the panel for the verification of its structural integrity and the sensor capabilities. The optical fibers were then used for the newly-developed PPP-BOTDA (Pulse-PrePump Brillouin Optical Time Domain Analysis) system. The long-range distributed strain and temperature can be measured by this system, whose spatial resolution is 100 mm. The strain changes from the FBGs and the PPP-BOTDA agreed well with those from the conventional strain gages and FE analysis in the CFRP panel. Therefore, the fiber-optic sensors and its system were very effective for the evaluation of the VaRTM composite structures.

Keywords

Health monitoring, fiber-optic sensors, non-destructive evaluation, VaRTM, CFRPs

1. Introduction

Applications of CFRPs into aircraft structures have markedly increased because it is accepted that these materials are very reliable and have the required properties of strength combined with light weight. Most composite structures are fabricated by prepregs, which are ready-to-mold materials in sheet form impregnated with resin.

* To whom correspondence should be addressed. E-mail: stakeda@chofu.jaxa.jp
Edited by the JSCM

DOI:10.1163/156855108X314760

The conventional fabrication process is especially costly for large-scale composite structures because of the many assembly steps and autoclave equipment. VaRTM (Vacuum-assisted Resin Transfer Molding) is a very promising molding method to take the place of the conventional molding method. In VaRTM, dry preforms are mounted to a one-sided mold and covered by a flexible bagging film where the cavity is sealed by vacuum tape. VaRTM offers the potential to reduce fabrication costs because it requires no expensive prepreg or autoclave equipment. In addition, VaRTM is effective for the integral molding of complex-shaped composite structures because the resin is impregnated into vacuum bagging with combined dry preforms. The low-cost composite materials made by VaRTM have already been used for many industrial applications, e.g. windmill blades and boats. To apply this type of material to aircraft structures, it is necessary to develop a novel VaRTM technology to guarantee higher mechanical properties and a more stable quality as well as a high fiber volume fraction of the composite material.

Our group has been conducting a research program related to VaRTM composite structures by a step-by-step approach [1]. This program has carried out many tests to evaluate the formability and mechanical properties of the material. First, we built a 2 m $\times$ 1 m flat-stiffened panel with two different shapes of stringers, a Z-shape and a hat-shape. Although this panel was fabricated integrally by VaRTM, high material quality and good mechanical properties were obtained from evaluation tests. Next, we built a 2 m long integral structure with a curved stiffened skin panel and spars to simulate a portion of the outer wing of a small-size civil aircraft. Conventional blade type stringers were adopted, which have the benefits of maintenance simplification and the elimination of actual structure inspection. This structure also includes some technical challenge elements, such as ply drop-off and a thick section around the access hole. The skin and spar web are tapered from a thick section to a thin section as a result of the ply drop-off. Some difficulties in the resin impregnation, namely, incomplete impregnation or partial dry spots, were found in the thick sections of the structure. Since they were caused by the low permeability of the present dry preform, the VaRTM process has to be improved to achieve better quality of the structure. Processing parameters such as the locations of resin inlets and outlets, flow sequence, and impregnation time were carefully selected so that the resin can flow into the mold and fill the preform completely. The internal conditions of vacuum bagging, strain, or temperature are also important for the molding. Hence, the sensing techniques are useful for good quality control of VaRTM composite structures.

Fiber-optic sensors are being used for some infrastructures to replace the point-to-point sensor system with the new sensing network because of their light weight and multiplexed capability. Since PPP-BOTDA (Pulse-PrePump Brillouin Optical Time Domain Analysis) and multiplexed FBGs (Fiber Bragg Gratings) can achieve wide-range sensing, they are suitable for the process monitoring and evaluation of the structural integrity in large-scale composite structures. In the previously described program, the monitorings using fiber-optic sensors have been applied as

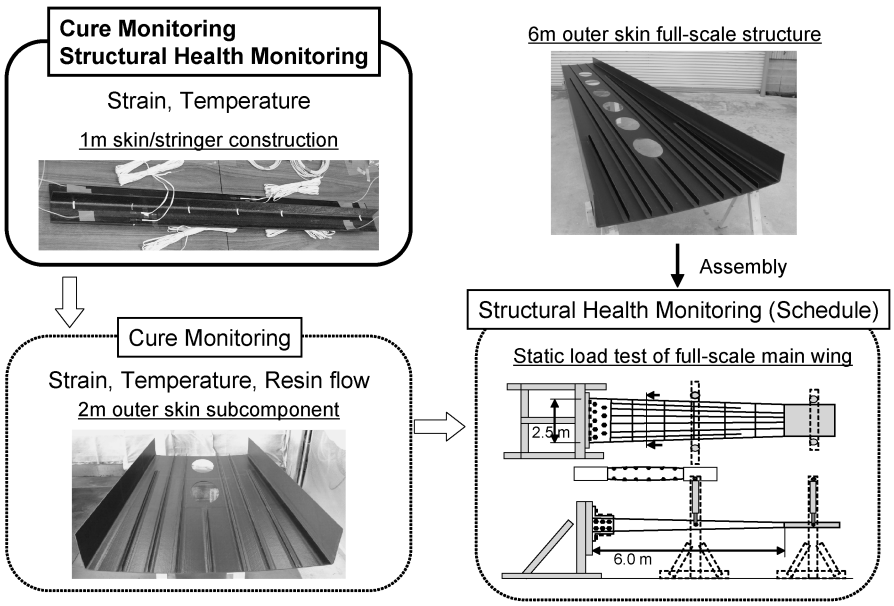

Figure 1. Research plan related to monitoring using fiber-optic sensors.

shown in Fig. 1. Among them, we report monitoring results of the curing process and the structural integrity for a CFRP-stiffened panel manufactured by VaRTM.

2. CFRP-Stiffened Panel

A stiffened panel was fabricated by VaRTM on the assumption that it is a partial structure of the outer skin of small-size civil aircrafts. As shown in Fig. 2, the panel combined the T-shaped stringer with a skin of 900 mm × 100 mm × 4.8 mm. The materials were dry preforms of UD carbon fabric (T800SC-24k, Saertex Co. KG) and epoxy resin (XNR6809/XNH6809, NagaseEleX. Co. Ltd.). The stacking sequences were $[45/0/-45/90]_{S3}$ for the skin and $[45/0/-45/90]_{S2}$ for the stringer. Since fiber-optic sensors were used for both the process monitoring and the structural health monitoring, small-diameter optical fibers were embedded into the interface between the skin part and the stringer part. The resin was impregnated into the vacuum bag, including the combined dry preforms and molding equipments at 40°C. After the confirmation of the impregnation, the resin was stored at 80°C in 6 h for the curing process. The post-curing was carried out at 120°C within 3 h.

Small-diameter FBG sensors (Hitachi Cable Ltd.) were applied to both the process monitoring and the structural health monitoring. Sensor locations were 180 mm away from the edge (FBG1) and the center (FBG2). Two FBG sensors were arranged on each location; one was a normal FBG for strain measurement and the other was a strain-free state FBG in the hollow tube for temperature measurement [2]. The single FBG sensor was fabricated in a single optical fiber as

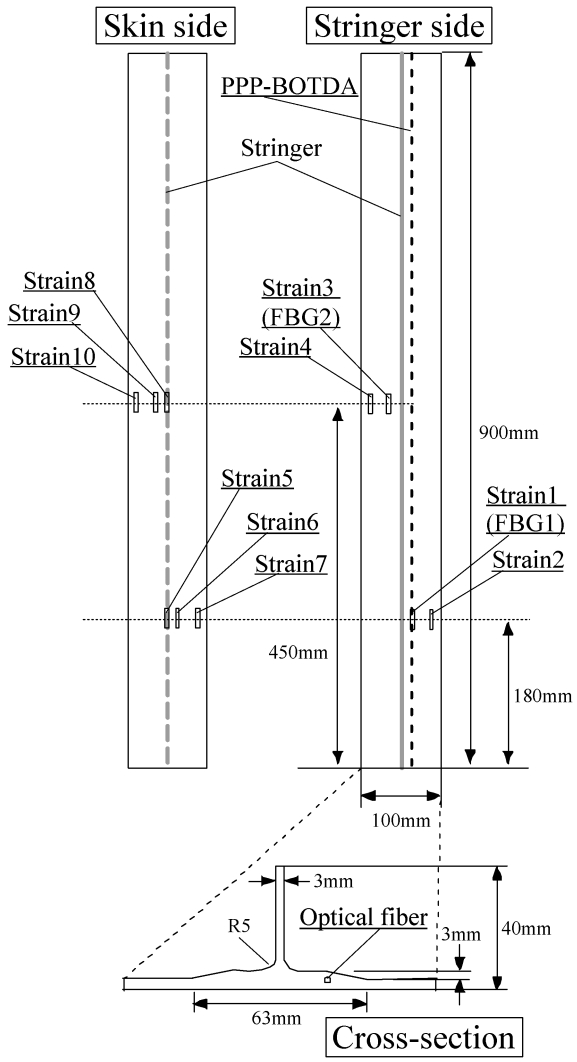

Figure 2. Illustration of composite skin/stringer panel.

a localized sensor, and its gauge length was 10 mm. After the process monitoring, the distributed sensing technique was applied to the structural health monitoring using PPP-BOTDA system (NBX-6000, Neubrex Co. Ltd.) for comparison of the results of the FBG sensors. A new technique of Pulse-PrePump is used for the PPP-BOTDA. This technique has improved some drawbacks of normal BOTDA, like dependence on optical fiber length or considerable increase in the signal noise level with the measuring distance. The PPP-BOTDA allows the achievement of cm-order spatial resolution and strain accuracy as high as 25 $\mu\varepsilon$ [3]. The power of Brillouin scattered light is quite small in such a long-range application because optical power loss occurs along the entire length of the optical fiber. The practical

power of the light source will be limited by the appearances of some non-linear phenomena [4]. Thus the optical power loss of the small-diameter optical fibers was also improved by the changes in the core diameter and the relative index difference. This kind of improvement becomes considerably important for embedded fiber-optic sensors into composites in the future. Electrical-resistance strain gauges were attached to the stringer side (from Strain1 to Strain4) and the skin side (from Strain5 to Strain10) as shown in Fig. 2. The strains were also measured by the strain gauges during the four-point bending as structural health monitoring. The strain values were used for comparison with the strain values calculated by the FE analysis of the panel, and for reference values under the four-point bending.

3. Process Monitoring of VaRTM

Strain and temperature are important physical values for the VaRTM process because they represent the cure state of the epoxy resin. An FBG sensor produces the reflected light measured as a reflection spectrum. Relationships between the center wavelength of the reflection spectrum and strain and/or temperature are known to be almost linear. These relationships are used for the strain and temperature measurements in this study. The reflection spectrum was measured by an optical spectrum analyzer at sampling speeds of 6/min, and the period of the process monitoring was all three days. The strain measurement accuracy and temperature measurement accuracy are 1 $\mu\varepsilon$ and 0.1°C, respectively.

Figure 3 shows the strain and temperature changes obtained by the measured reflection spectra. The strain was compensated by the FBG for temperature measurement because the temperature transition is relatively large compared to the strain change in the fabrication process. When the dry preform of the stringer was

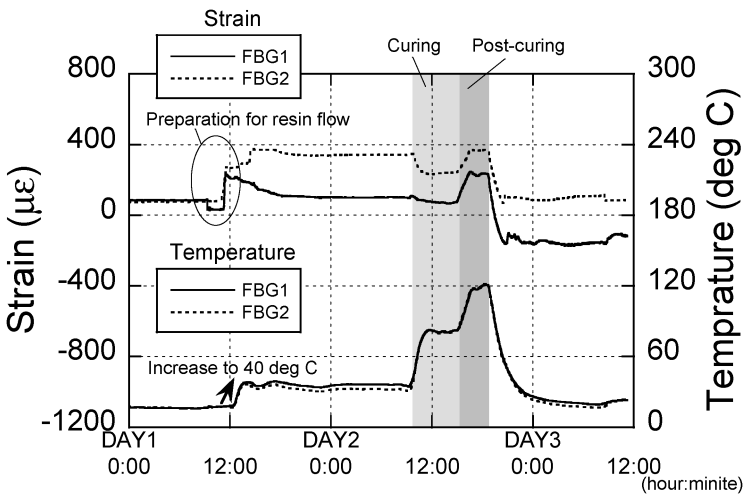

Figure 3. Strains and temperatures measured by FBG sensors.

put on the dry preform of the skin before 12:00 of DAY1, the FBG sensors were able to detect the strain changes sensitively. Since a slight loading was applied to the FBG sensors due to the positioning of the dry preforms, the strains changed into about 250 $\mu\varepsilon$ for both the FBG1 and the FBG2. As the processing temperature increased from room temperature (22°C) to 40°C, the temperature compensation will be effective because the strain changes were small. During the constant temperature process of the 40°C, the strain values were different, such as 350 $\mu\varepsilon$ and 100 $\mu\varepsilon$. This is because the applied slight bending or twist differ between the two FBG sensors, and this will influence the strain values. When the processing temperature is increased from 40°C to 80°C, the strains decreased due to cure shrinkage. Moreover, with further increase in the processing temperature from 80°C to 120°C, the strains were expected to increase due to expansion of the epoxy resin. The strain difference between FBG1 and FBG2 before the curing process remained till after the post-curing process or final stage of the fabrication process.

Comparison between temperature measured by the FBG sensors and temperature measured by thermocouples is shown in Fig. 4. TC1, TC2 and TC3 denote the temperatures measured by the thermocouples. The locations of temperature measurement were outside of the vacuum bagging (TC1) and inside of the vacuum bagging (TC2 and TC3). At the curing process from 9:30 to 15:00 of DAY2, the temperatures of TC1 and TC3 indicated an overshoot of the set value, 80°C. At the post-curing process from 15:00 to 19:00 of DAY2, the temperature of TC3 also indicated an overshoot of the set value, 120°C. Nevertheless, the temperatures measured by the FBG sensors were in good agreement with those measured by the thermocouples. On the other hand, the temperature changes measured by the FBG slowed down compared with those measured by the thermocouples. This time-lag was caused by the embedding of the FBG sensors into the dry preform because the speed of heat transfer was relatively low. Since internal temperature directly

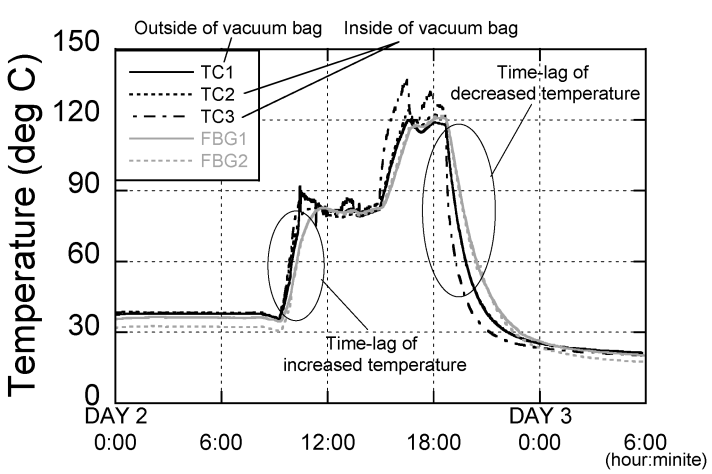

Figure 4. Temperatures measured by thermocouples and FBG sensors.

affects the resin curing, the temperature measured by the FBG sensors are useful for the fabrication process including temperature control. The composite panel of this study was a small substructure, however, so the monitoring is more useful for large-scale composite structures that are easily affected by temperature distribution depending on the location.

4. Structural Health Monitoring Under Four-Point Bending

4.1. Experimental Results

After the fabrication, the CFRP skin/stringer panel was cut out to test four-point bending as shown in Fig. 5. The quasi-static loading was applied to the panel at a displacement control of 0.5 mm/min. The test appearance and the boundary conditions are shown in Fig. 5. The strain changes were monitored by the embedded FBG sensors and the distributed sensing technique, PPP-BOTDA. The loading value, the displacement at the center of the panel, and the strain values measured by conventional strain gages were obtained simultaneously. In the PPP-BOTDA system, strain measurement accuracy and spatial resolution are ± 25 $\mu\varepsilon$ and 0.1 m, respectively. Since it takes one or two minutes to measure the distributed strain like other distributed sensing techniques, the loading was maintained at the strain values of 500 $\mu\varepsilon$ and 1000 $\mu\varepsilon$ in Strain10 of Fig. 2. The load–deflection curve for the loading–unloading period is shown in Fig. 6. The relationship between load and deflection was almost linear until Strain10 increased to 1000 $\mu\varepsilon$. Maximum deflection and bending load were 9.78 mm and -2.85 kN, respectively.

Figure 7 shows the distributed strains along the optical fiber direction. The results of the measured strains contain some external noise because not only the embedded part into the panel but also the entire optical fiber serve as the distributed sensing

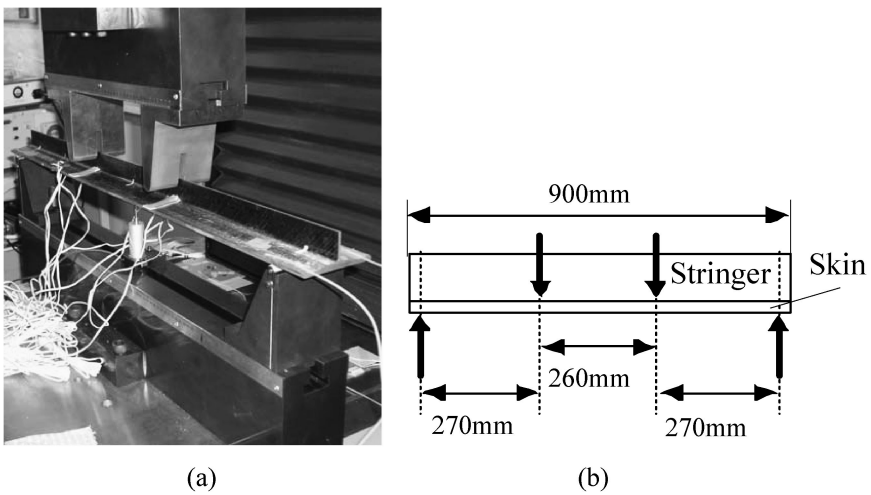

Figure 5. Quasi-static four-point bending test. (a) Test appearance and (b) boundary condition.

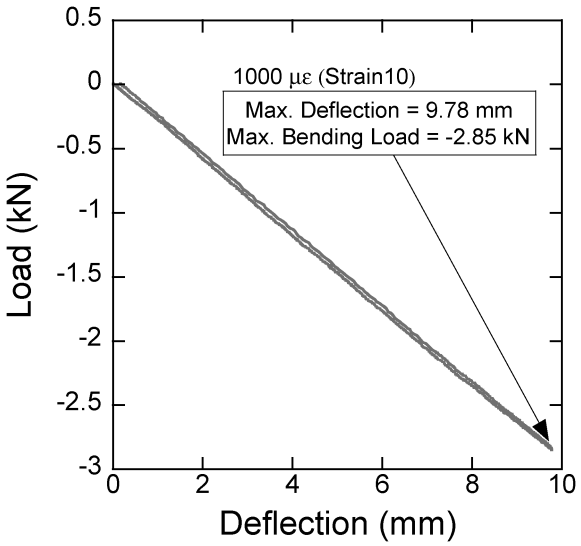

Figure 6. Load–deflection curve during bending test.

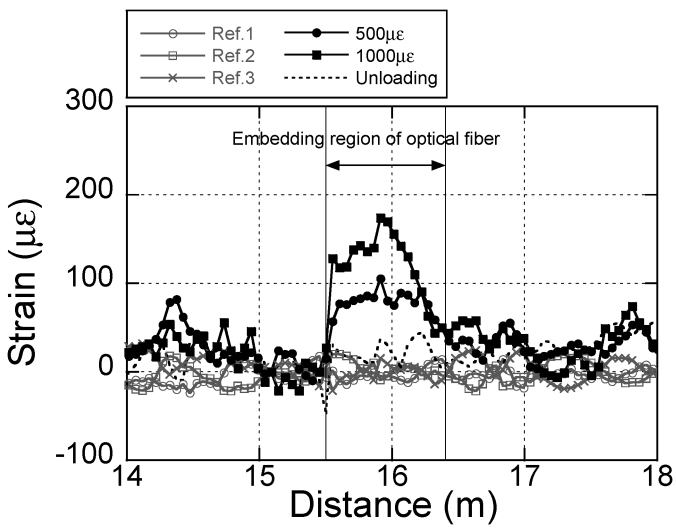

Figure 7. Strains measured by PPP-BOTDA.

network. Thus, three results of the strain measurements at the strain-free state were used for the averaging procedure as shown in Ref. 1, Ref. 2 and Ref. 3 of Fig. 7. Though the strain values fluctuated around 0 με before the loading, the embedding can be monitored due to the loading till Strain10 reaches 500 με. When the additional loading was applied to the panel, the value of Strain10 was confirmed to reach 1000 με.

Table 1.
Strains measured by FBG sensors and PPP-BOTDA

Applied strain ($\mu\varepsilon$)	FBG1 ($\mu\varepsilon$)	FBG2 ($\mu\varepsilon$)	PPP-BOTADA ($\mu\varepsilon$)
500	49	101	76 (FBG1) 105 (FBG2)
100	89	201	119 (FBG1) 174 (FBG2)

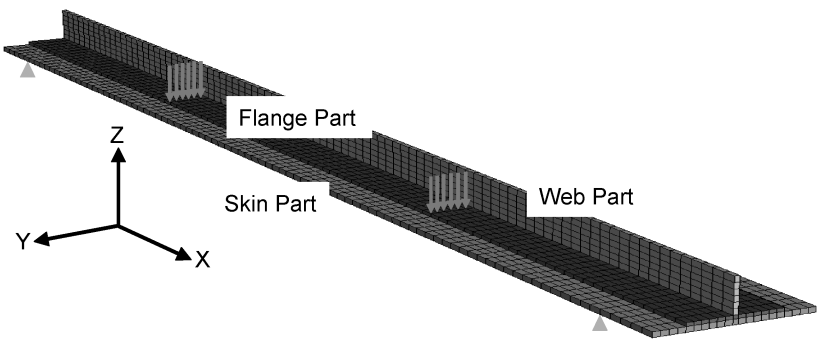

Figure 8. FE model of skin/stringer panel.

The strain values measured by the FBG sensors, and the strain values at the same locations as the FBG sensors measured by the PPP-BOTDA are summarized in Table 1. The strain values were very small because the embedding locations are close to the neutral axis of the panel. As a result, there were differences between the strains measured by the FBG and the PPP-BOTDA, which were caused by the slight changes in embedding locations, the difference in strain measurement techniques and the difference in the strain accuracies. However, comparable increasing and decreasing tendencies were observed experimentally.

4.2. FE Analysis

For verification of the validities of measured strains, the skin/stringer panel was modeled by using an 8-node continuum shell element as shown in Fig. 8. A full FE model is required because the panel is made from the UD fabric exhibiting anisotropy. Thus, such a shell element is suited to the laminated composites for the saving of calculation cost [5]. The FE model consisted of three different plates: skin part, flange part and web part. The total number of elements and nodes were 3620 and 7826, respectively. Table 2 shows the mechanical properties of the CFRP for the calculation. The calculated strain was obtained under the conditions of 500 $\mu\varepsilon$ and 1000 $\mu\varepsilon$ in Strain10 of Fig. 2. The FE analysis was performed by using ABAQUS code. X-direction strain distributions at the surface of each part are shown in Fig. 9.

Table 2.
Mechanical properties of the CFRP for FE analysis

E_X (GPa)	154
E_Y (GPa)	7.8
N_{XY}	0.354
G_{XY} (GPa)	4.0

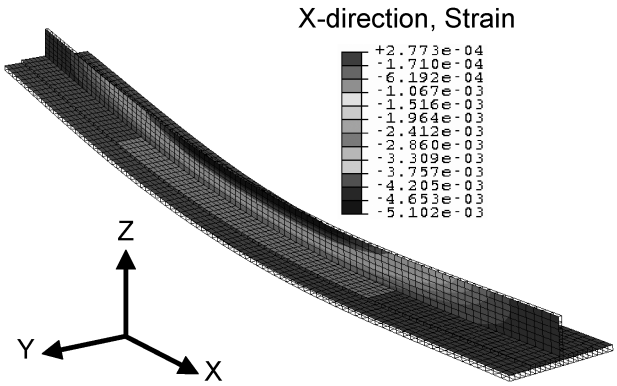

Figure 9. *X*-direction strain distributions at surface of each part.

The compressive strain was calculated at both the web part between the upper indenting tools and the flange part just below the upper indenting tools. Even though the upper surface of the skin part is usually under a compressive strain condition, this was more than 0 $\mu\varepsilon$ due to the stiffness of the web part. Time–strain curves at the skin side are shown in Fig. 10(a). The two-stage constant strain areas corresponded to 500 $\mu\varepsilon$ and 1000 $\mu\varepsilon$ in the Strain10. Strain gauges around FBG1 (Strains5, 6, 7) indicate small strain changes compared with strain gauges around FBG2 (Strains8, 9, 10). Figure 10(b) shows the calculated strain distribution in the lower 45° layer of the skin part under the condition of 1000 $\mu\varepsilon$ in Strain10. Since strain gauges are attached to the lower surface of the skin part, measured strains could be confirmed by this distribution. Time–strain curves at the stringer side are shown in Fig. 11(a). Strain gauges on the skin part (Strains2, 4) indicated tensile strain, while strain gauges on the flange part (Strain3) indicated compressive strain. These different strain changes can be confirmed by calculated strain distributions in the upper 45° layer of the skin part and the flange part under the condition of 1000 $\mu\varepsilon$ in Strain10.

All the strain values are summarized in Table 3. The measured strains are small compared with the calculated strains for the results of Strain1 and Strain3. This is because the gradient of the thickness in the flange part could not be introduced into the FE model and the attached location of the strain gauges was on the borderline of the thickness change. Using the calculated results, the measured strains were

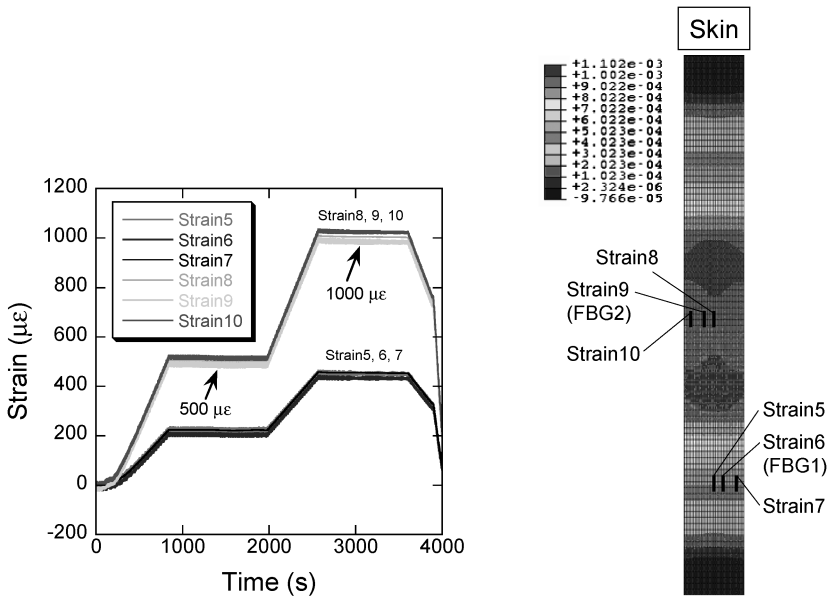

Figure 10. Measured and calculated strains at skin side. (a) Time–strain curves and (b) calculated strain distribution.

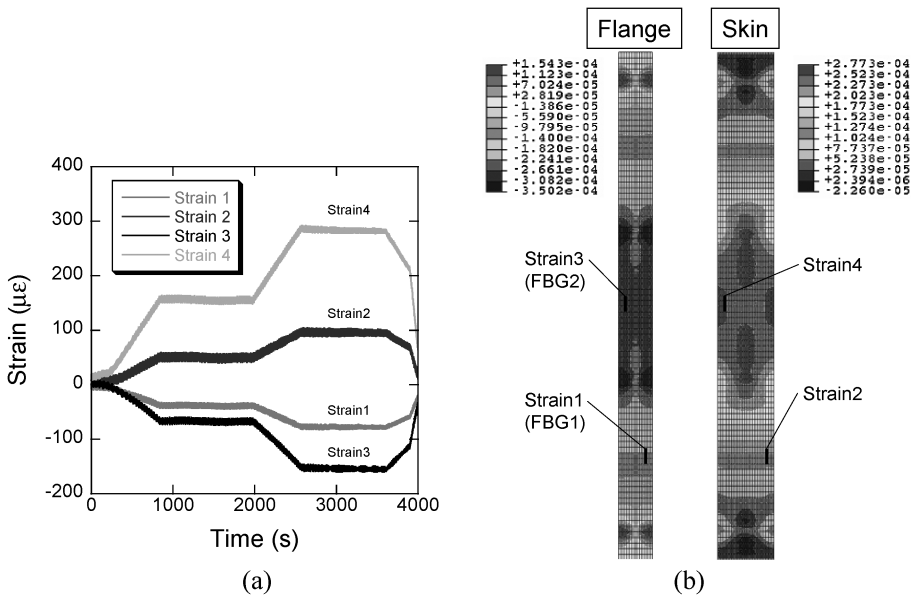

Figure 11. Measured and calculated strains at stringer side. (a) Time–strain curves and (b) calculated strain distributions.

Table 3.
Comparison of measured and calculated strains

	Measured strain (με)	Calculated strain (με)
FBG1 (PPP-BOTDA)	89 (119)	114
FBG2 (PPP-BOTDA)	201 (174)	236
Strain1	−82	−130
Strain2	104	121
Strain3	−160	−268
Strain4	293	253
Strain5	464	483
Strain6	443	483
Strain7	458	482
Strain8	1010	1001
Strain9	1000	1000
Strain10	1036	1000

verified for the strain gauges and the embedded FBG sensors. The corresponding strain to the embedded FBG sensor was assumed to be the same as the average of the stain in the upper 45° layer of the skin part and the strain in the lower 45° layer of the flange part. The strains measured by the fiber-optic sensors were in good agreement with those of calculated strains. The embedded FBG sensors and optical fibers for the PPP-BOTDA were verified to be useful for the structural health monitoring as well as the process monitoring of VaRTM.

5. Conclusions

A CFRP-stiffened panel was fabricated by VaRTM for the monitoring of the molding process including measurements of strain and temperature using FBG sensors. Four-point bending was applied to the panel for verification of its structural integrity and the sensor capabilities using the FBG sensors and the PPP-BOTDA system. Though the economic efficiency has to be considered for practical use, the monitoring with fiber-optic sensors was found to be effective for increasing VaRTM composite structures. The following are issues in the future of health monitoring using fiber-optic sensors:

- FBG sensors: cost of multiplexing, reproducibility of embedding condition;
- PPP-BOTDA: strain accuracy and spatial distance, processing time of measurement.

Acknowledgement

We would like to thank Neubrex Co. Ltd. for the distributed strain measurement with the PPP-BOTDA system.

References

1. Y. Nagao, T. Nakamura, J. Nakamichi and T. Ishikawa, in: *Proc 9th Japan Intl SAMPE Sympos.*, pp. 163–166 (2005) in CD-ROM.
2. T. Mizutani, K. Hayashi, N. Takeda, F. Namiki and K. Tanaka, in: *Proc. 2nd JSME/ASME Intl Conf. Materials and Processing* (2005) in CD-ROM.
3. K. Kishida, L. Che-Hien and K. Nishiguchi, in: *Proc. SPIE 17th Intl Conf. Optical Fibre Sensors*, Vol. 5855, pp. 559–562 (2005).
4. G. P. Agrawal, *Nonlinear Fiber Optics*. Academic Press, San Diego, USA (1995).
5. ABAQUS Version 6.5 Analysis User's Manual, 15.6.2-3.